Potent neuroprotection after stroke afforded by a double-knot spider-venom peptide that inhibits acid-sensing ion channel 1a

Irène R. Chassagnon[a], Claudia A. McCarthy[b,c], Yanni K.-Y. Chin[a], Sandy S. Pineda[a], Angelo Keramidas[d], Mehdi Mobli[e], Vi Pham[b,c], T. Michael De Silva[b,c], Joseph W. Lynch[d], Robert E. Widdop[b,c], Lachlan D. Rash[a,f,1], and Glenn F. King[a,1]

[a]Institute for Molecular Bioscience, The University of Queensland, St. Lucia, QLD 4072, Australia; [b]Biomedicine Discovery Institute, Monash University, Clayton, VIC 3800, Australia; [c]Department of Pharmacology, Monash University, Clayton, VIC 3800, Australia; [d]Queensland Brain Institute, The University of Queensland, St. Lucia, QLD 4072, Australia; [e]Centre for Advanced Imaging, The University of Queensland, St. Lucia, QLD 4072, Australia; and [f]School of Biomedical Sciences, The University of Queensland, St. Lucia, QLD 4072, Australia

Edited by Solomon H. Snyder, Johns Hopkins University School of Medicine, Baltimore, MD, and approved February 6, 2017 (received for review September 1, 2016)

Stroke is the second-leading cause of death worldwide, yet there are no drugs available to protect the brain from stroke-induced neuronal injury. Acid-sensing ion channel 1a (ASIC1a) is the primary acid sensor in mammalian brain and a key mediator of acidosis-induced neuronal damage following cerebral ischemia. Genetic ablation and selective pharmacologic inhibition of ASIC1a reduces neuronal death following ischemic stroke in rodents. Here, we demonstrate that Hi1a, a disulfide-rich spider venom peptide, is highly neuroprotective in a focal model of ischemic stroke. Nuclear magnetic resonance structural studies reveal that Hi1a comprises two homologous inhibitor cystine knot domains separated by a short, structurally well-defined linker. In contrast with known ASIC1a inhibitors, Hi1a incompletely inhibits ASIC1a activation in a pH-independent and slowly reversible manner. Whole-cell, macropatch, and single-channel electrophysiological recordings indicate that Hi1a binds to and stabilizes the closed state of the channel, thereby impeding the transition into a conducting state. Intracerebroventricular administration to rats of a single small dose of Hi1a (2 ng/kg) up to 8 h after stroke induction by occlusion of the middle cerebral artery markedly reduced infarct size, and this correlated with improved neurological and motor function, as well as with preservation of neuronal architecture. Thus, Hi1a is a powerful pharmacological tool for probing the role of ASIC1a in acid-mediated neuronal injury and various neurological disorders, and a promising lead for the development of therapeutics to protect the brain from ischemic injury.

stroke | acid-sensing ion channel 1a | venom peptide | neuroprotection | ischemia

Most strokes (>85%) are ischemic (1–3), and the disruption of blood flow that occurs during cerebral ischemia leads to neuronal damage in localized vascular territories within a few minutes (4). Whether blood flow is completely or partially impeded defines two distinct regions of tissue damage, known as the core and penumbral (peri-infarct) zones, respectively (1–3, 5). The core tissue exposed to the most dramatic reduction in blood flow is mortally injured and thought to undergo irreversible necrotic cell death (2). In contrast, the ischemic penumbra, which can compose up to one-half of the total lesion volume during the initial stages of ischemia, undergoes apoptosis over a period of hours to days, and thus is potentially salvageable via poststroke therapy (2). With time, the infarct core expands into the ischemic penumbra, and this therapeutic opportunity is lost (1, 6).

Oxygen depletion during cerebral ischemia compels the brain to switch from oxidative phosphorylation to anaerobic glycolysis. The resultant acidosis causes the extracellular pH to fall from ∼7.3 to 6.0–6.5 in the ischemic core under normoglycemic conditions, and it can fall to below 6.0 during severe ischemia under hyperglycemic conditions (7, 8). The pH for half-maximal activation (pH_{50}) of acid-sensing ion channel 1a (ASIC1a) in human cortical neurons is 6.6 (9), and, consequently, these channels are robustly activated by the decrease in extracellular pH that occurs during cerebral ischemia. ASIC1a is the primary acid sensor in mammalian brain (9, 10) and a key mediator of stroke-induced neuronal damage. Genetic ablation of ASIC1a reduces infarct size by ∼60% after transient middle cerebral artery occlusion (MCAO) in mice (7), whereas pharmacologic blockade with modestly potent ASIC1a inhibitors, such as amiloride (7) and nonsteroidal anti-inflammatory drugs (11), yield less robust neuroprotection.

The most potent inhibitor of ASIC1a identified to date is psalmotoxin 1 (PcTx1), a 40-residue peptide isolated from venom of the tarantula *Psalmopoeus cambridgei*. PcTx1 inhibits rat ASIC1a (rASIC1a) with IC_{50} ∼1 nM without inhibiting other ASIC subtypes (12, 13). Intracerebroventricular (i.c.v.) administration of a single small dose of PcTx1 (1 ng/kg) at 2 h after MCAO in rats reduced cortical infarct volume by ∼70% and greatly improved behavioral outcomes (14). Intranasal administration of *P. cambridgei* venom at 2–4 h after MCAO in mice reduced infarct volume by ∼50% (15), although how much of this affect can be attributed to the inhibition of ASIC1a is unclear, given that PcTx1 represents only ∼0.4% of total venom protein (14). Neither PcTx1 nor any other ASIC inhibitor has been shown to provide significant neuroprotection beyond 2–4 h after stroke onset. Here, we describe the isolation and characterization of a venom peptide that potently inhibits

Significance

Six million people die each year from stroke, and 5 million survivors are left with a permanent disability. Moreover, the neuronal damage caused by stroke often triggers a progressive decline in cognitive function that doubles the risk of dementia for stroke survivors. Despite this massive global disease burden, there are no approved drugs for treating the neuronal injury caused to the brain by the oxygen deprivation occurring during an ischemic stroke. The precipitous drop in brain pH resulting from stroke activates acid-sensing ion channel 1a. We show that inhibition of these channels using a "double-knot" spider venom peptide massively attenuates brain damage after stroke and improves behavioral outcomes, even when the peptide is administered 8 h after stroke onset.

Author contributions: I.R.C., C.A.M., A.K., J.W.L., R.E.W., L.D.R., and G.F.K. designed research; I.R.C., C.A.M., Y.K.-Y.C., S.S.P., A.K., M.M., V.P., T.M.D.S., L.D.R., and G.F.K. performed research; I.R.C., C.A.M., Y.K.-Y.C., S.S.P., A.K., J.W.L., R.E.W., L.D.R., and G.F.K. analyzed data; and I.R.C., C.A.M., R.E.W., L.D.R., and G.F.K. wrote the paper.

Conflict of interest statement: The authors' universities (The University of Queensland and Monash University) have jointly filed a patent application that covers use of the peptides described in this article (Hi1a–Hi1d).

This article is a PNAS Direct Submission.

Data deposition: The atomic coordinates and structure factors have been deposited in the Protein Data Bank, www.pdb.org (PDB ID code 2N8F). The NMR chemical shift assignments have been deposited in the BioMagResBank (accession no. 25848).

[1]To whom correspondence may be addressed. Email: l.rash@uq.edu.au or glenn.king@imb.uq.edu.au.

This article contains supporting information online at www.pnas.org/lookup/suppl/doi:10.1073/pnas.1614728114/-/DCSupplemental.

ASIC1a via a unique mode of action and protects the brain from neuronal injury when administered up to 8 h after stroke onset.

Results

Discovery of Hi1a. Analysis of a venom-gland transcriptome from the Australian funnel-web spider *Hadronyche infensa* (Fig. 1*A*) revealed a family of four peptides with marked similarity to PcTx1, the prototypical ASIC1a inhibitor from an unrelated spider (12). In contrast to PcTx1, these peptides are larger (75–77 residues), and comprise two tandem PcTx1-like sequences joined by a short linker (Fig. 1*B*). The N- and C-terminal regions of the most abundantly expressed family member, Hi1a, have 62% and 50% identity with PcTx1, respectively, suggesting that these peptides evolved through duplication of a gene encoding a PcTx1-like toxin. Production of recombinant Hi1a by overexpression in *Escherichia coli* yielded a single dominant isomer with six disulfide bonds (Fig. S1). Two-electrode voltage-clamp (TEVC) recordings revealed that Hi1a potently inhibits both rASIC1a and human ASIC1a (hASIC1a) expressed in *Xenopus* oocytes (IC_{50} values of 0.40 and 0.52 nM, respectively) but never inhibits >80% of ASIC1a currents even at saturating doses (Fig. 1 *C* and *D*). At 1 μM, Hi1a had no effect on rASIC2a or rASIC3 and only mildly potentiated rASIC1b, indicative of >2,000-fold higher potency for rASIC1a over these other subtypes (Fig. 1*E*). PcTx1 (10 nM) completely inhibited ASIC1a, but the effect was rapidly reversible on peptide washout (τ_{off} = 6.2 min for rASIC1a, 0.99 min for hASIC1a; Fig. 1*F* and Fig. S2). In striking contrast, current inhibition by 10 nM Hi1a was only slowly reversible (τ_{off} = 14.2 min for rASIC1a, 31.8 min for hASIC1a), with ~40% recovery of current amplitude after a 30-min washout (Fig. 1*F* and Fig. S2). Such slow reversibility has not been reported for any other ASIC modulator.

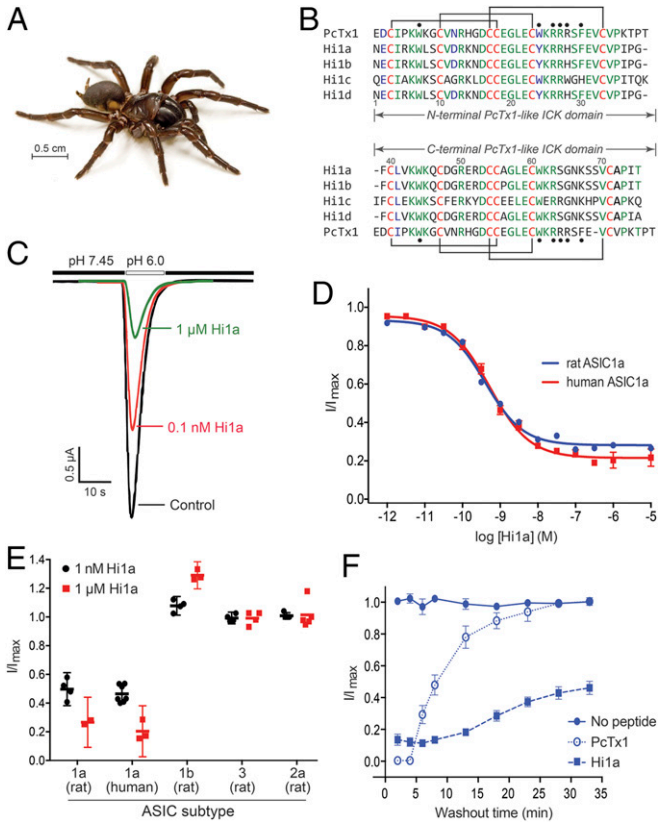

Fig. 1. Hi1a selectively inhibits ASIC1a. (*A*) Australian funnel-web spider *H. infensa*. Photo courtesy of Bastian Rast, ArachnoServer database (43). (*B*) Sequence alignment of PcTx1 with members of the Hi1a family. Identical and highly conserved residues are shown in green and blue, respectively, except for conserved cysteine residues, which are in red. The disulfide framework of PcTx1 is shown above and below the alignment. Black circles denote pharmacophore residues of PcTx1 (13, 20). (*C*) Representative current traces from *Xenopus* oocytes expressing rASIC1a in the absence (black) or presence (red and green) of Hi1a. Currents were evoked by a pH drop from 7.45 to 6.00. Note the incomplete current inhibition at a saturating concentration of Hi1a (1 μM). (*D*) Concentration-response curves for Hi1a inhibition of rASIC1a (blue) and hASIC1a (red). Fitting a Hill equation to the data yielded IC_{50} values of 0.40 ± 0.08 nM and 0.52 ± 0.06 nM, respectively. Data are mean ± SEM; n = 8. (*E*) Effect of 1 nM (black) and 1 μM (red) Hi1a on homomeric ASICs expressed in *Xenopus* oocytes. Hi1a has >2,000-fold selectivity for ASIC1a over these subtypes. Data are mean ± SEM; n = 5. (*F*) Recovery of rASIC1a currents following inhibition by Hi1a and PcTx1. Oocytes expressing rASIC1a were exposed to 10 nM PcTx1 or Hi1a at pH 7.45 for 120 s twice. Whole-cell currents were elicited by rapid switching from pH 7.45 to 6.00 every 60 s (and every 5 min following washout). Data are mean ± SEM; n = 5.

Hi1a Inhibits Activation of ASIC1a. PcTx1 binds to the acidic pocket of ASIC1a (16, 17), a key proton-binding site on the channel (18), and promotes steady-state desensitization (SSD) (19). In contrast to PcTx1, which causes a surmountable shift in the pH dependence of activation and SSD to more alkaline values (19), Hi1a-induced inhibition is substantially less pH-dependent, as evidenced by only small alkaline shifts in the pH_{50} of SSD in the absence and presence of peptide, and this effect is insurmountable (Fig. 2*A* and Fig. S3*A*). In addition, in contrast to PcTx1, Hi1a induced a small acidic shift (0.18 pH units at 5 nM for hASIC1a; Fig. S3*A*) and a noncompetitive inhibition of ASIC1a activation. Thus, despite the remarkable sequence similarity between PcTx1 and Hi1a, particularly in the N-terminal PcTx1-like domain, which contains many of the key pharmacophore residues of PcTx1 (Fig. 1*B*) (13, 20), Hi1a has substantially different functional activity, as demonstrated by its incomplete, pH-independent inhibition and slow off-rate.

To further explore Hi1a's unique mode of action, we obtained macropatch and single-channel recordings of hASIC1a overexpressed in HEK293 cells in the absence and presence of a saturating concentration of Hi1a (5 nM). The macropatch recordings revealed that Hi1a induced a marked reduction of peak current (78.6%; Fig. 2*B*) and a fivefold decrease in the rate of hASIC1a activation. In contrast, the rates of desensitization and current deactivation were barely affected (Fig. S3*B*). In single-channel recordings, pre-exposure to Hi1a markedly increased the activation lag time after acidification from 3.4 ms to 22 ms (Fig. 2*C*). In contrast, all-points amplitude histograms revealed that the current amplitude remained unchanged at 1.0 pA after Hi1a exposure, suggesting that Hi1a does not affect ion permeation (Fig. 2*D*). Analysis of the distributions of shut and open dwell times of single-channel activity revealed additional, long-lived components for both shut and open distributions after exposure to Hi1a (Fig. S3*C*).

Taken together, our TEVC, macropatch, and single-channel data demonstrate that Hi1a induces a delay in the activation of ASIC1a, suggesting that it binds to and stabilizes the closed state of the channel. This is a strikingly different mode of action from that of PcTx1, which stabilizes the desensitized state of ASIC1a (19, 21). From these data, we infer that Hi1a slows the conformational rearrangements of ASIC1a that underlie its transition from the resting state to a conducting state.

Hi1a Is a Double-Knot Peptide. The structure of PcTx1 (13, 16, 17, 22) reveals that it forms an inhibitor cystine knot (ICK) motif that is common in spider venom peptides and typically provides them with a high degree of thermal and chemical stability, as well as resistance to proteases (23). The solution structure of Hi1a, which we determined using a heteronuclear NMR approach (24), shows that it comprises two homologous ICK domains connected via a short and structurally well-defined linker (Fig. 3 *A* and *B* and Table S1). Thus, Hi1a is a member of the recently described "double-knot" toxin family (25). The β-hairpin loop is precisely defined in the C-terminal ICK domain but is more disordered in the N-terminal domain, as has been noted for the β-hairpin loop of PcTx1 (13), which houses most of the pharmacophore residues (20). Because each ICK domain has both sequence and structural similarity with PcTx1, we produced recombinant versions of the N-terminal (Hi1a:N) and C-terminal (Hi1a:C) ICK domains and tested whether they are active in isolation (Fig. 3 *C* and *D*). Hi1a:N induced full inhibition of ASIC1a, but with markedly reduced potency (IC_{50} ~200-fold greater than that for either PcTx1 or Hi1a). Moreover, in contrast with full-length Hi1a, this weak inhibition was rapidly

PHARMACOLOGY

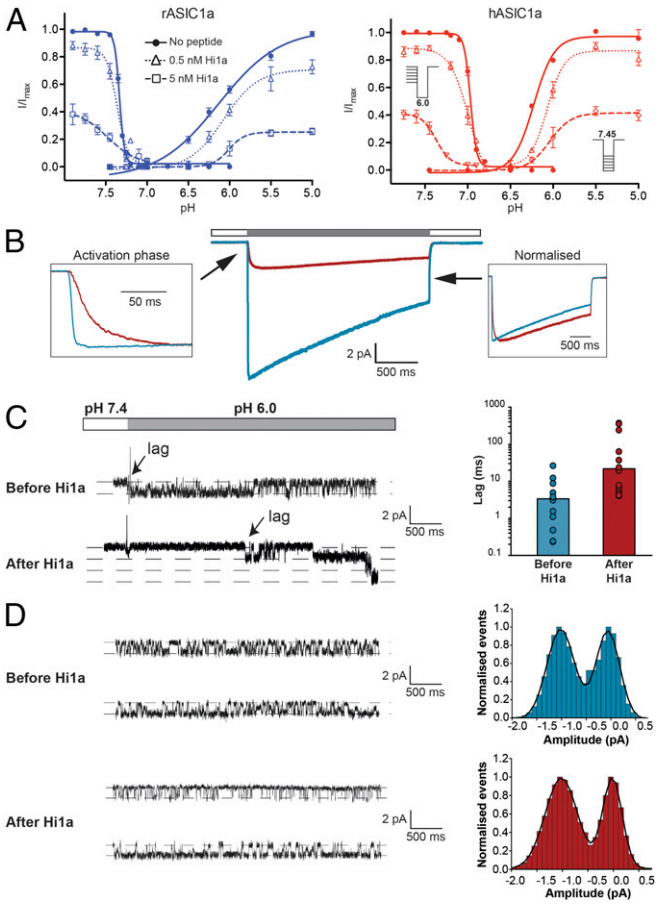

Fig. 2. Hi1a inhibits ASIC1a activation. (*A*) Effect of Hi1a on the pH-dependence of activation and SSD of rASIC1a (*Left*) and hASIC1a (*Right*). Activation curves were obtained by applying increasing concentrations of protons every 50 s. In the continued presence of protons (pH <~7.2 for rASIC1a), ASICs rapidly desensitize and cannot reopen until sufficiently deprotonated (pH >~7.3 for rASIC1a), a phenomenon known as SSD. SSD profiles were obtained by conditioning the channels for 120 s at decreasing pH. Data are mean ± SEM; $n = 6$. (*B*) Representative macropatch recordings from HEK293 cells expressing hASIC1a before (blue) and after (red) exposure to 5 nM Hi1a for 2 min. (*Insert, Left*) Expanded view of activation phase showing that Hi1a causes a marked reduction in the rate of current activation. (*Insert, Right*) Normalized deactivation phase currents showing that Hi1a has no significant effect on current deactivation. (*C*) Representative single-channel recording showing rapid activation of hASIC1a following a pH drop from 7.45 to 6.00 (*Left, Middle*). The lag time before channel activation is markedly increased in the presence of 5 nM Hi1a (*Left, Bottom*). (*Right*) Distribution of activation lag times before and after exposure to Hi1a ($n = 10$). *$P < 0.001$. (*D, Left*) Representative single-channel recordings before (*Top*) and after (*Bottom*) application of 5 nM Hi1a. (*D, Right*) Corresponding all-points amplitude histograms showing that Hi1a has no effect on hASIC1a current amplitude (~1.0 pA).

reversible (Fig. 3*F*). Hi1a:C did not inhibit ASIC1a at all; rather, at concentrations >1 μM, the C-terminal ICK domain caused minor potentiation of channel currents.

Because Hi1a resembles two concatenated PcTx1-like domains, we asked whether simply linking two copies of PcTx1 would recapitulate the unique activity of Hi1a. An engineered peptide containing two copies of PcTx1 joined by a short linker inhibited rASIC1a ~200-fold less potently than Hi1a (IC_{50} ~63 nM; Fig. 3*E*). Moreover, like PcTx1, but in contrast to Hi1a, this engineered double-knot peptide induced full inhibition of ASIC1a currents. However, a chimeric double-knot peptide comprising an N-terminal PcTx1 fragment joined to the C-terminal ICK domain of Hi1a (PcTx1-Hi1a:C) potently inhibited ASIC1a (IC_{50} 1.27 nM; Fig. 3*E*), and, in contrast with PcTx1 and the double-PcTx1 peptide, caused incomplete inhibition, similar to that induced by Hi1a. We conclude that the unique mechanism of action of Hi1a requires covalent linkage of the two ICK domains, with the C-terminal domain imparting the unusual property of incomplete channel inhibition at saturating peptide concentrations.

Residue F350 in rASIC1a is located on α-helix 5 adjacent to an acidic pocket that is critical for proton gating of the channel (18). Mutation of this residue to Ala abolishes the ability of PcTx1 to inhibit ASIC1a (26). Similarly, we found that Hi1a was inactive on an F350A mutant of rASIC1a (Fig. 3*G*), suggesting that the binding sites for PcTx1 and Hi1a on ASIC1a overlap at least partly. Binding of Hi1a at the acidic pocket is consistent with our hypothesis that the peptide impedes the conformational rearrangements necessary for the resting channel to transition into a conducting state.

Hi1a Protects the Brain After Stroke. Because PcTx1 protects against stroke (14, 15), and Hi1a inhibits ASIC1a with higher potency and slower reversibility than PcTx1, we investigated the neuroprotective efficacy of Hi1a both in vitro and in vivo. In primary neuron/astrocyte cultures that

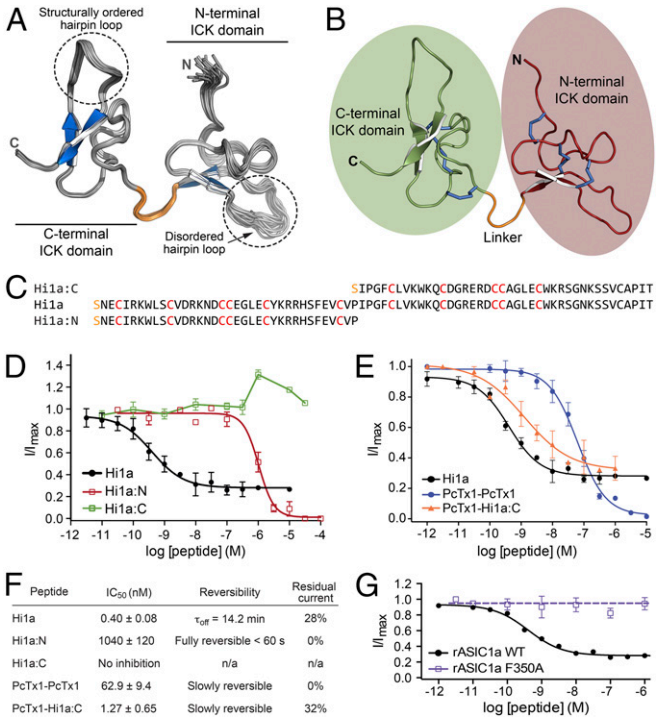

Peptide	IC_{50} (nM)	Reversibility	Residual current
Hi1a	0.40 ± 0.08	τ_{off} = 14.2 min	28%
Hi1a:N	1040 ± 120	Fully reversible < 60 s	0%
Hi1a:C	No inhibition	n/a	n/a
PcTx1-PcTx1	62.9 ± 9.4	Slowly reversible	0%
PcTx1-Hi1a:C	1.27 ± 0.65	Slowly reversible	32%

Fig. 3. Hi1a is a double-knot peptide, with unique activity requiring both knots. (*A*) Solution structure of Hi1a (ensemble of 20 structures; PDB ID code 2N8F). A structured linker (orange) separates two closely apposed ICK domains. The β-hairpin loop in each ICK domain is highlighted. (*B*) Schematic of top-ranked structure from the Hi1a ensemble highlighting the N- and C-terminal ICK domains (red and green), linker (orange), and six disulfide bridges (blue). (*C*) Sequence alignment of recombinant Hi1a and recombinant Hi1a:N and Hi1a:C domains. The N-terminal serine residue (orange) is a vestige of the fusion protein cleavage site. (*D*) Concentration-response curves showing the effects of full-length Hi1a and Hi1a:N and Hi1a:C domains on rASIC1a. Hi1a:N fully inhibited rASIC1a, but with low potency (IC_{50} >1 μM), whereas Hi1a:C did not inhibit rASIC1a. Data are mean ± SEM; $n = 6$. (*E*) Effect of engineered double-knot peptides on rASIC1a. A peptide composed of two linked copies of PcTx1 fully inhibited rASIC1a with moderate potency (IC_{50} 62.9 ± 9.4 nM; blue). In contrast, a chimeric double-knot peptide composed of an N-terminal PcTx1 domain joined to the C-terminal ICK domain of Hi1a (PcTx1-Hi1a:C) inhibited rASIC1a with similar potency as wild-type Hi1a (IC_{50} = 1.27 ± 0.65 nM; orange), and also caused incomplete inhibition at saturating concentrations. Data are mean ± SEM. PcTx1-PcTx1, $n = 11$; PcTx1-Hi1a:C, $n = 6$. (*F*) Pharmacologic properties of each peptide when tested against rASIC1a. Residual current is the percentage of pH-induced current remaining at a saturating concentration of peptide. Data are mean ± SEM; $n = 6$. (*G*) Concentration-dependent effects of Hi1a on wild-type and mutant (F350A) rASIC1a expressed in *Xenopus* oocytes.

were oxidatively stressed with 0.3 mM H_2O_2, both PcTx1 and Hi1a caused concentration-dependent increases in cell viability (Fig. S4); however, at the highest concentration tested (100 nM), Hila provided greater neuroprotection than PcTx1, with cell viability of 77% and 68%, respectively (Fig. S4).

We next investigated the neuroprotective efficacy of Hi1a in a rat model of focal cerebral ischemia. Stroke was induced in conscious, spontaneously hypertensive rats (SHRs) by titrating endothelin-1 (ET-1) above the right middle cerebral artery (MCA) via an indwelling cannula to cause vessel occlusion and evoke stroke-induced behavior (14). This vasoconstrictive stroke model more closely resembles human stroke than mechanical occlusion models (3). A single small dose of Hi1a (2 ng/kg) administered i.c.v. at 2, 4, or 8 h after stroke caused a marked reduction in infarct size (Fig. 4 *A* and *B*). Strikingly, Hi1a afforded protection not only in the penumbral (cortical) zone, but also in the ischemic (striatal) core, which is the tissue directly impacted by hypoxia and is generally considered refractory to therapeutic intervention (2). These findings are consistent with the preservation of neuronal architecture in both the penumbral and core regions of damage, as evidenced by intact neuronal staining (Fig. 4*E*), and were reflected symptomatically, with the Hi1a-treated animals exhibiting markedly reduced neurological deficit (Fig. 4*C*) and motor impairment (Fig. 4*D*).

The neuroprotective efficacy of Hi1a is not due simply to an ability to cause vasodilation, because it did not modify the ET-1–evoked vasoconstriction of isolated cerebral arteries even at concentrations as high as 100 nM (Fig. S5*A*). Vascular tone in Hi1a-treated arteries was similar to that in time controls, despite the fact that these vessels fully dilated in response to the vasodilator papaverine (Fig. S5*B*).

Discussion

Hi1a Provides a Long Time Window for Neuroprotection After Stroke. Stroke is the second-leading cause of death worldwide (27) and the primary cause of serious long-term disability (28), with treatment of stroke accounting for ∼3% of global healthcare expenditures (29). Despite this massive disease burden, the use of tissue plasminogen activator (tPA) to help restore blood flow remains the only Food and Drug Administration-approved agent for treatment of ischemic stroke. Moreover, tPA is used in only 3–4% of stroke patients (30), owing to its relatively narrow therapeutic window and the risk of inducing intracranial hemorrhage (1, 31). Currently, there are no approved therapeutic agents for treating the neuronal damage caused by stroke (5). Neuroprotective drugs would need to have long time window for therapeutic efficacy, given that ∼60% of stroke patients do not reach an emergency room until at least 2 h after stroke onset (3), and many patients do not receive medical care until much later.

In this study, we have demonstrated that inhibition of ASIC1a using Hi1a provides exceptional levels of neuroprotection even when the peptide is administered up to 8 h after stroke onset. Along with facilitating a substantially reduced level of penumbral damage, Hi1a is unique in providing some protection of the striatal core region, which is generally considered therapeutically unrecoverable owing to rapid and irreversible necrotic cell death (2). Importantly, we have shown that the reduction in infarct volume in Hi1a-treated animals translates to improved behavioral outcomes, with a marked decrease in neurological deficits and motor impairment. We observed no adverse effects during the 72-h observation period following i.c.v. administration of Hi1a, consistent with previous work showing that central or peripheral administration of ASIC inhibitors does not produce unwanted side effects (32).

Mechanistic Basis of Hi1a's Neuroprotective Efficacy. Hi1a is the most potent inhibitor of ASIC1a described to date; its IC_{50} of ∼500 pM for the inhibition of both rASIC1a and hASIC1a makes it approximately twofold more potent than PcTx1. Hi1a comprises two ICK domains that have strong sequence homology with PcTx1, and its 3D structure resembles two concatenated PcTx1 molecules joined by a structured linker. Both peptides are highly neuroprotective in MCAO models of stroke. Despite these similarities, Hi1a and PcTx1 have distinctly different mechanisms of action. PcTx1 binds to the acidic pocket of ASIC1a to promote desensitization of the channel (19). In contrast, although the binding site for Hi1a overlaps with that of PcTx1 (Fig. 3*G*), Hi1a delays the activation of ASIC1a (Fig. 2), suggesting that it binds to and stabilizes the closed state of the channel. Moreover, Hi1a causes incomplete channel block even at saturating peptide concentrations, and its inhibition of ASIC1a is less readily reversible than that of PcTx1. The slower reversibility of Hi1a, as well as its pH-independent inhibition of ASIC1a, may provide a greater "effective dose" than an equivalent amount of PcTx1 over a range of extracellular conditions, whereas the residual channel activity even at saturating doses of Hi1a might be important for retaining normal physiological functions of brain ASIC1a, which remain unclear.

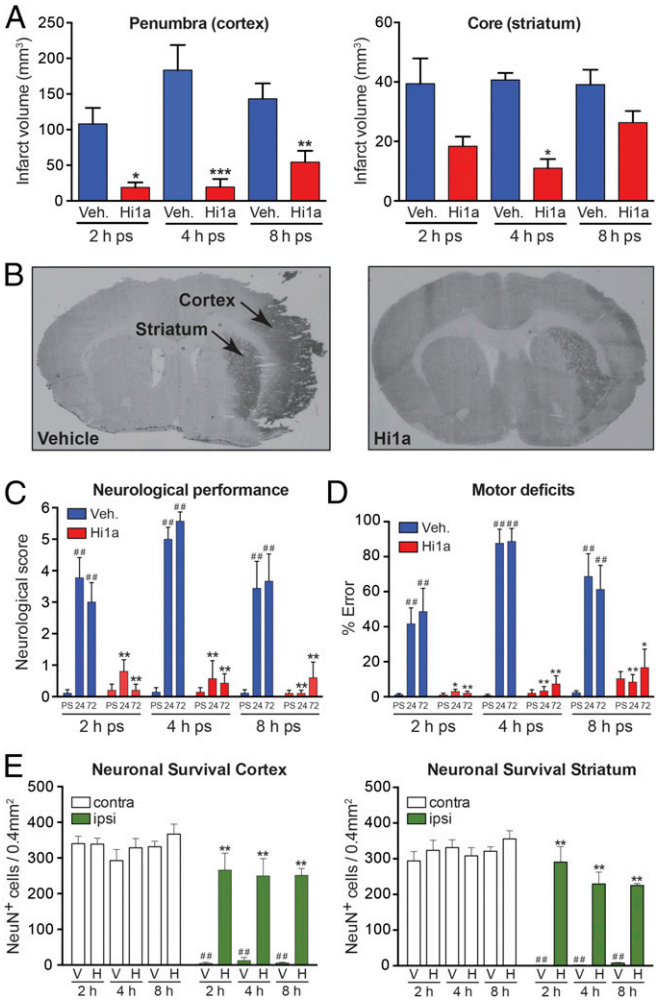

Fig. 4. Hi1a is highly neuroprotective in a realistic model of human stroke. (*A*) Infarct volumes in penumbral (cortical) and core (striatal) regions of damage following MCAO in conscious rats. Rats were administered i.c.v. vehicle (saline, blue) or Hi1a (2 ng/kg, red) at 2, 4, or 8 h poststroke (ps). Vehicle: 2 h, $n = 10$; 4 h, $n = 7$; 8 h, $n = 9$. Hi1a: 2 h, $n = 5$; 4 h, $n = 7$; 8 h, $n = 10$. Volumes were measured at 72 h poststroke and corrected for edema. $^*P < 0.05$, $^{**}P < 0.01$, $^{***}P < 0.001$ vs. vehicle (one-way ANOVA). (*B*) Coronal sections showing typical infarcted (darker area) and noninfarcted regions from rats treated with either vehicle or Hi1a (2 ng/kg) at 8 h after stroke. (*C*) Neurologic scores measured prestroke (PS) and at 24–72 h poststroke (ps). $^{\#\#}P < 0.01$ vs. prestroke performance; $^{**}P < 0.01$ vs. corresponding time in vehicle-treated group (two-way repeated-measures ANOVA followed by Tukey post hoc tests). (*D*) Motor score (% error in ledged beam test) measured prestroke and at 24–72 h poststroke. $^{\#\#}P < 0.01$ vs. prestroke performance; $^*P < 0.05$, $^{**}P < 0.01$ vs. corresponding time in vehicle treated group (two-way repeated-measures ANOVA followed by Tukey post hoc tests). (*E*) Neuronal survival in cortical (*Left*) and striatal (*Right*) regions measured at 72 h poststroke. Data are expressed as number of NeuN-immunopositive ($NeuN^+$) cells per 0.4 mm^2 within occluded (ipsilateral) and nonoccluded (contralateral) hemispheres. $^{**}P < 0.01$ vs. vehicle-treated group (ipsilateral side); $^{\#\#}P < 0.01$ vs. matched region on noninfarcted hemisphere (two-way ANOVA followed by Tukey post hoc tests). All data are mean ± SEM.

PHARMACOLOGY

Hi1a was neuroprotective even when administered 8 h after onset of ET-1–mediated MCAO. Although we did not determine the degree and duration of ET-1–mediated cerebral ischemia, previous studies have reported either complete or partial recovery of blood flow at 8 h after stroke (33–35). In this context, we have shown that the neuroprotection afforded by Hi1a is unlikely to result from a vasodilatory effect, given that it did not reverse ET-1–mediated vasoconstriction of isolated cerebral arteries.

It was recently shown that acidosis induces neuronal necroptosis via direct association of activated ASIC1a with RIP1 kinase independent of ASIC1a's ion-conducting function (36), consistent with RIP1's function as a crucial mediator of necroptosis (37). An indirect effect of Hi1a on RIP1 activation might explain its ability to provide some protection of the striatal region, which is thought to undergo rapid necrotic cell death following cerebral ischemia. However, pharmacological inhibition of RIP1 only marginally reduces infarct size (~15%) at 6 h after MCAO (38), whereas Hi1a provides much higher levels of protection at up to 8 h after stroke induction. Thus, it remains to be determined whether inhibition of RIP1 recruitment contributes to the neuroprotective efficacy of Hi1a. In future preclinical studies, it also will be critical to examine stroke outcomes over several weeks, to ensure that the neuroprotective effects of Hi1a are not transient.

Materials and Methods

Analysis of the *H. infensa* Transcriptome. Three specimens of *H. infensa* were collected from Orchid Beach, Fraser Island, Australia and milked exhaustively to induce transcription of toxin genes. Three days later, the spiders were anesthetized, and venom glands were dissected into TRIzol (Life Technologies). Total RNA was extracted using standard methods, then mRNA enrichment was performed using an Oligotex Direct mRNA Mini Kit (Qiagen). RNA quality and concentration were determined using a Bioanalyzer 2100 instrument (Agilent Technologies), and 100 ng of mRNA was used to prepare a cDNA library. Sequencing was performed at the Australian Genome Research Facility using a Roche GS FLX sequencer. Low-quality sequences were discarded using a Phred score cutoff of 25. De novo assembly was performed using MIRA (39), and the data were visualized using Tablet (40) or Geneious (41). Signal sequences were identified using SignalP (42), and propeptide cleavage sites were predicted based on a sequence logo analysis of spider toxin precursors in the ArachnoServer database (43).

Production of Recombinant Peptides. Hi1a and analogs were produced using an *E. coli* periplasmic expression system developed for disulfide-rich peptides (44). In brief, a synthetic gene encoding the peptide was subcloned into an expression vector that enables periplasmic expression of the peptide as a His_6-MBP fusion protein, with a tobacco etch virus (TEV) protease cleavage site sandwiched between the MBP and peptide-coding regions (44). *E. coli* BL21 (λDE3) cells transformed with the vector were grown at 30 °C, induced with 0.5 mM isopropyl β-D-1-thiogalactopyranoside at OD_{600} = 0.8–1.3, then grown overnight at 16 °C. After cell disruption at 32 kpsi (TS Series Cell Disrupter; Constant Systems), the His_6-MBP-peptide fusion protein was captured by passing the cell lysate (buffered in 20 mM Tris·HCl and 200 mM NaCl, pH 7.8) over Ni-NTA Superflow Resin (Qiagen). The resin was washed with 10 mM imidazole to remove weakly bound contaminants, after which the fusion protein was eluted with 400 mM imidazole, concentrated to 5 mL, and then cleaved overnight at room temperature with TEV protease. The liberated recombinant peptide was then isolated to >95% purity using reversed-phase HPLC. Note that for all peptides, a nonnative serine residue was added at the N terminus to facilitate TEV cleavage.

NMR. The structure of Hi1a was determined from heteronuclear NMR data acquired at 25 °C on a Bruker 900-MHz spectrometer equipped with a triple-resonance cryogenic probe using a sample of $^{13}C/^{15}N$-labeled Hi1a [300 μM in 20 mM Mes, 0.02% NaN_3, and 5% (vol/vol) D_2O]. Backbone resonance assignments were obtained from 2D ^{1}H-^{15}N-HSQC, 2D ^{1}H-^{13}C-HSQC, 3D HNCACB, 3D CBCA(CO)NH, 3D HNCO, and 3D HBHA(CO)NH spectra, whereas side chain assignments relied on a 4D HCC(CO)NH-TOCSY (45). The 3D and 4D spectra were acquired using nonuniform sampling and processed using maximum entropy reconstruction (45). Chemical shift assignments have been deposited in BioMagResBank (accession no. 25848). Distance restraints for structure calculations were derived from 3D ^{13}C-aliphatic, ^{13}C-aromatic, and ^{15}N-edited NOESY-HSQC spectra (mixing time, 200 ms) acquired using uniform sampling. SPARKY (www.cgl.ucsf.edu/home/sparky/) was used for peak picking and integration of NOESY spectra, and then peak lists were assigned and structures calculated using CYANA 3.0 (46). Disulfide-bond connectivities were determined unambiguously in the first round of structure calculations, and corresponding disulfide-bond restraints (47) were applied in subsequent rounds. Backbone dihedral-angle restraints derived from TALOS+ (48) were also used in structure calculations. CYANA was used to calculate 200 structures from random starting conformations; then the 20 conformers with highest stereochemical quality as judged by MolProbity (49) were selected to represent the structure of Hi1a. Coordinates for the Hi1a ensemble are available from the Protein Data Bank (PDB ID code 2N8F).

TEVC. The TEVC experiments were carried out using *Xenopus laevis* oocytes expressing rat or human ASICs (13, 20). Stage V-VI oocytes were injected with 4 ng of cRNA encoding rASIC1a, hASIC1a, rASIC1b, rASIC2a, or rASIC3, and recordings were made 1–5 d later at room temperature (18–21 °C) in ND96 solution containing 0.05% fatty acid-free BSA. Changes in extracellular pH were induced using a microperfusion system that allowed local, rapid exchange of solutions. Hepes was replaced by Mes to buffer the pH 6.0 stimulus solution. The control extracellular solution comprised 96 mM NaCl, 2 mM KCl, 1.8 mM $CaCl_2$, 2 mM $MgCl_2$, and 5 mM Hepes. Peptides were dissolved in ND96 solution (pH 7.45) containing 0.05% BSA to prevent adsorption onto tubing.

Single-Channel Recordings. HEK293 cells were transfected with cDNA encoding hASIC1a. Recordings were performed at 22 ± 1 °C at a clamped potential of −70 mV, in the outside-out patch patch-clamp configuration. The intracellular solution comprised 145 mM CsCl, 2 mM $CaCl_2$, 2 mM $MgCl_2$, 10 mM Hepes, and 5 mM EGTA, adjusted to pH 7.4 with CsOH. The control extracellular solution comprised 140 mM NaCl, 5 mM KCl, 2 mM $CaCl_2$, 1 mM $MgCl_2$, 10 mM Hepes, and 10 mM D-glucose, adjusted to pH 7.4 with NaOH. The activating extracellular solution was identical to the control, except that 10 mM Mes was used instead of Hepes and the solution was titrated to pH 6.0 with NaOH. All working solutions also contained 0.01% BSA. Macropatch currents were generated by rapidly switching solutions across the patch using a piezoelectric stepper (rise time, ~150 μs). Single-channel and macropatch currents were recorded using an Axon 200B amplifier (Molecular Devices), filtered (–3 dB, four-pole Bessel) at 5 kHz, and sampled at 20 kHz. Macropatch currents were analyzed using pClamp10 (Molecular Devices). Between 10 and 20 macropatch currents were elicited from the same patch and averaged for measurement of rise, desensitization, and deactivation times. Group means were tested for significance using a paired *t* test, with $P < 0.01$ as the significance threshold. Activation lag time estimates represent median and 25th and 75th percentile values.

The 10–100% region of the rising phase of the current was fitted to the exponential equation $I(t) = I_{max}\,[1 - \exp(-t/\tau)]$, where I_{max} is the peak current amplitude, τ is the time constant, and t is time. A single standard exponential equation was used to fit the desensitization phase of the current. Two standard exponential equations fit the deactivation phase of the current, and a weighted time constant was calculated using the equation $\tau_w = (\tau_1 A_1 + \tau_2 A_2)/(A_1 + A_2)$, where τ_w is the weighted time constant for current deactivation and τ_n and A_n are individual time constants and corresponding fractions, respectively. Single-channel currents were analyzed using pClamp 10 and QuB. Shut and open dwell histograms were generated from idealized single-channel currents at a resolution (dead time) of 100 μs and fitted to a mixture of exponentials.

In Vitro Neuroprotection Assay. Oxidative stress was induced in primary cortical neuronal-astrocytic cultures by incubation with 0.3 mM H_2O_2. Then cell viability in the presence/absence of Hi1a or PcTx1 (1–100 nM) was assessed using a colorimetric assay. More details are provided in Fig. S4.

Stroke Experiments. We used a focal reperfusion model of stroke in conscious SHRs (14). Two 23-gauge stainless steel guide cannulae were stereotaxically implanted into anesthetized animals (ketamine 75 mg/kg; xylazine 10 mg/kg i.p.) at 5 d before stroke induction. The first cannula was implanted 3 mm dorsal to the right MCA for stroke induction. The second cannula was implanted into the left lateral ventricle for drug administration. After 5 d of recovery, stroke was induced by inserting a 30-gauge injector protruding 3 mm below the previously implanted cannula and administering ET-1 (20 pmol/μL) at a rate of 0.2 μL every 30 s until the animal exhibited stroke-induced behaviors, including continuous ipsilateral circling, clenching, dragging, failure to extend the left contralateral forelimb, chewing, jaw flexing, and shuffling with forepaws (level 4 stroke). These motor deficits correlate with stroke severity (50) and provide a consistent benchmark for stroke induction in conscious rats. Only animals that achieved a level 4 stroke were included in the study. Animals that showed behaviors exceeding a level 4 stroke (e.g., complete loss of balance, excessive spinning) were excluded and humanely euthanized. Animals that had a rectal temperature >40 °C during the 3 h after stroke induction, lost >10% body weight, failed to feed and drink, or lacked spontaneous movement were

excluded as well. Animals were randomly allocated to vehicle or Hi1a treatment group before the initiation of stroke induction and the experimenter (C.M.) was blinded to all treatments and histological analyses. At 2, 4, or 8 h after stroke, SHRs were treated with a single i.c.v. dose of Hi1a (2 ng/kg) or saline using a 30-gauge injector protruding 3 mm below the guide cannula. Drugs were dissolved in saline and infused in a volume of 3 μL over 3 min.

Stroke-induced motor deficit was assessed by counting foot faults while the rat traversed a gradually narrowing ledged beam (14, 50). Animals were trained to traverse the beam on 2 consecutive days before prestroke assessment. Postural abnormalities were assessed by elevating the rat by the tail above a flat surface and grading the severity of thorax twisting and angle of forelimb extension. These indicators of neurologic health were scored between 0 and 3, with a score of 0 corresponding to no twisting of the thorax or complete forelimb extension toward the flat surface, and a score of 3 corresponding to severe thorax twisting and failure to extend the forelimb. The scores for thorax twisting and forelimb extension were summed to give a total possible neurologic score of 6, which represents severe neurologic deficit. Behavioral tests were performed before stroke and at 24 and 72 h after stroke. At 72 h poststroke, rats were reanesthetized (ketamine 75 mg/kg; xylazine 10 mg/kg i.p.) and transcardially perfused with physiologically buffered saline. Brains were removed, snap-frozen, and sectioned (16 μm) at eight predetermined forebrain levels (–3.20 mm to 6.8 mm relative to bregma). Sections were imaged, and infarct volumes were measured in all brain sections using the ballistic light method and corrected for edema (14, 50).

Cerebral Artery Vascular Tone. Brains were rapidly removed from euthanized male SHR and placed in artificial cerebrospinal fluid. A distal segment of the MCA (109 ± 10 μm; $n = 7$ arteries) was isolated and transferred to a pressure myograph chamber (Living Systems Instrumentation). Vessels were cannulated and pressurized to 60 mmHg. After a 30-min equilibration period, vessels were submaximally constricted (~25% of postequilibration diameter) with ET-1 (1–10 nM). Cumulative concentration-response curves were then performed to either vehicle (0.9% saline) or Hi1a (1–100 nM). Arteries were then treated with papaverine (100 μM) to obtain maximum diameters.

ACKNOWLEDGMENTS. We thank the Queensland NMR Network for providing access to its 900-MHz NMR spectrometer. This work was supported by Australian National Health and Medical Research Council Principal Research Fellowship (to G.F.K.) and Project Grant APP1063798 (to G.F.K. and R.E.W.); Australian Research Council Future Fellowship (to M.M.); and The University of Queensland International Postgraduate Research Scholarship (to I.R.C.).

1. Moskowitz MA, Lo EH, Iadecola C (2010) The science of stroke: Mechanisms in search of treatments. *Neuron* 67(2):181–198.
2. Woodruff TM, et al. (2011) Pathophysiology, treatment, and animal and cellular models of human ischemic stroke. *Mol Neurodegener* 6(1):11.
3. Wey HY, Desai VR, Duong TQ (2013) A review of current imaging methods used in stroke research. *Neurol Res* 35(10):1092–1102.
4. Choi DW, Rothman SM (1990) The role of glutamate neurotoxicity in hypoxic-ischemic neuronal death. *Annu Rev Neurosci* 13:171–182.
5. Liu R, Yuan H, Yuan F, Yang SH (2012) Neuroprotection targeting ischemic penumbra and beyond for the treatment of ischemic stroke. *Neurol Res* 34(4):331–337.
6. Richard Green A, Odergren T, Ashwood T (2003) Animal models of stroke: Do they have value for discovering neuroprotective agents? *Trends Pharmacol Sci* 24(8):402–408.
7. Xiong ZG, et al. (2004) Neuroprotection in ischemia: Blocking calcium-permeable acid-sensing ion channels. *Cell* 118(6):687–698.
8. Isaev NK, et al. (2008) Role of acidosis, NMDA receptors, and acid-sensitive ion channel 1a (ASIC1a) in neuronal death induced by ischemia. *Biochemistry (Mosc)* 73(11):1171–1175.
9. Li M, et al. (2010) Acid-sensing ion channels in acidosis-induced injury of human brain neurons. *J Cereb Blood Flow Metab* 30(6):1247–1260.
10. Wemmie JA, et al. (2003) Acid-sensing ion channel 1 is localized in brain regions with high synaptic density and contributes to fear conditioning. *J Neurosci* 23(13):5496–5502.
11. Mishra V, Verma R, Raghubir R (2010) Neuroprotective effect of flurbiprofen in focal cerebral ischemia: The possible role of ASIC1a. *Neuropharmacology* 59(7-8):582–588.
12. Escoubas P, et al. (2000) Isolation of a tarantula toxin specific for a class of proton-gated Na^+ channels. *J Biol Chem* 275(33):25116–25121.
13. Saez NJ, et al. (2011) A dynamic pharmacophore drives the interaction between psalmotoxin-1 and the putative drug target acid-sensing ion channel 1a. *Mol Pharmacol* 80(5):796–808.
14. McCarthy CA, Rash LD, Chassagnon IR, King GF, Widdop RE (2015) PcTx1 affords neuroprotection in a conscious model of stroke in hypertensive rats via selective inhibition of ASIC1a. *Neuropharmacology* 99:650–657.
15. Pignataro G, Simon RP, Xiong ZG (2007) Prolonged activation of ASIC1a and the time window for neuroprotection in cerebral ischaemia. *Brain* 130(Pt 1):151–158.
16. Dawson RJ, et al. (2012) Structure of the acid-sensing ion channel 1 in complex with the gating modifier psalmotoxin 1. *Nat Commun* 3:936.
17. Baconguis I, Gouaux E (2012) Structural plasticity and dynamic selectivity of acid-sensing ion channel-spider toxin complexes. *Nature* 489(7416):400–405.
18. Jasti J, Furukawa H, Gonzales EB, Gouaux E (2007) Structure of acid-sensing ion channel 1 at 1.9 Å resolution and low pH. *Nature* 449(7160):316–323.
19. Chen X, Kalbacher H, Gründer S (2005) The tarantula toxin psalmotoxin 1 inhibits acid-sensing ion channel (ASIC) 1a by increasing its apparent H^+ affinity. *J Gen Physiol* 126(1):71–79.
20. Saez NJ, et al. (2015) Molecular dynamics and functional studies define a hot spot of crystal contacts essential for PcTx1 inhibition of acid-sensing ion channel 1a. *Br J Pharmacol* 172(20):4985–4995.
21. Chen X, Kalbacher H, Gründer S (2006) Interaction of acid-sensing ion channel (ASIC) 1 with the tarantula toxin psalmotoxin 1 is state dependent. *J Gen Physiol* 127(3):267–276.
22. Escoubas P, Bernard C, Lambeau G, Lazdunski M, Darbon H (2003) Recombinant production and solution structure of PcTx1, the specific peptide inhibitor of ASIC1a proton-gated cation channels. *Protein Sci* 12(7):1332–1343.
23. King GF, Hardy MC (2013) Spider-venom peptides: Structure, pharmacology, and potential for control of insect pests. *Annu Rev Entomol* 58:475–496.
24. Bende NS, et al. (2014) A distinct sodium channel voltage-sensor locus determines insect selectivity of the spider toxin Dc1a. *Nat Commun* 5:4350.
25. Bohlen CJ, et al. (2010) A bivalent tarantula toxin activates the capsaicin receptor, TRPV1, by targeting the outer pore domain. *Cell* 141(5):834–845.
26. Sherwood T, et al. (2009) Identification of protein domains that control proton and calcium sensitivity of ASIC1a. *J Biol Chem* 284(41):27899–27907.
27. Feigin VL, et al.; Global Burden of Diseases, Injuries, and Risk Factors Study 2010 (GBD 2010) and the GBD Stroke Experts Group (2014) Global and regional burden of stroke during 1990-2010: Findings from the Global Burden of Disease Study 2010. *Lancet* 383(9913):245–254.
28. Stapf C, Mohr JP (2002) Ischemic stroke therapy. *Annu Rev Med* 53:453–475.
29. Evers SM, et al. (2004) International comparison of stroke cost studies. *Stroke* 35(5):1209–1215.
30. Besancon E, Guo S, Lok J, Tymianski M, Lo EH (2008) Beyond NMDA and AMPA glutamate receptors: Emerging mechanisms for ionic imbalance and cell death in stroke. *Trends Pharmacol Sci* 29(5):268–275.
31. Chapman SN, et al. (2014) Current perspectives on the use of intravenous recombinant tissue plasminogen activator (tPA) for treatment of acute ischemic stroke. *Vasc Health Risk Manag* 10:75–87.
32. Baron A, et al. (2013) Venom toxins in the exploration of molecular, physiological and pathophysiological functions of acid-sensing ion channels. *Toxicon* 75:187–204.
33. Biernaskie J, Corbett D, Peeling J, Wells J, Lei H (2001) A serial MR study of cerebral blood flow changes and lesion development following endothelin-1–induced ischemia in rats. *Magn Reson Med* 46(4):827–830.
34. Mecca AP, O'Connor TE, Katovich MJ, Sumners C (2009) Candesartan pretreatment is cerebroprotective in a rat model of endothelin-1–induced middle cerebral artery occlusion. *Exp Physiol* 94(8):937–946.
35. Glendenning ML, Lovekamp-Swan T, Schreihofer DA (2008) Protective effect of estrogen in endothelin-induced middle cerebral artery occlusion in female rats. *Neurosci Lett* 445(2):188–192.
36. Wang YZ, et al. (2015) Tissue acidosis induces neuronal necroptosis via ASIC1a channel independent of its ionic conduction. *eLife* 4:e05682.
37. Christofferson DE, Li Y, Yuan J (2014) Control of life-or-death decisions by RIP1 kinase. *Annu Rev Physiol* 76:129–150.
38. Degterev A, et al. (2005) Chemical inhibitor of nonapoptotic cell death with therapeutic potential for ischemic brain injury. *Nat Chem Biol* 1(2):112–119.
39. Chevreux B, et al. (2004) Using the miraEST assembler for reliable and automated mRNA transcript assembly and SNP detection in sequenced ESTs. *Genome Res* 14(6):1147–1159.
40. Milne I, Bayer M, Stephen G, Cardle L, Marshall D (2016) Tablet: Visualizing next-generation sequence assemblies and mappings. *Methods Mol Biol* 1374:253–268.
41. Kearse M, et al. (2012) Geneious Basic: An integrated and extendable desktop software platform for the organization and analysis of sequence data. *Bioinformatics* 28(12):1647–1649.
42. Bendtsen JD, Nielsen H, von Heijne G, Brunak S (2004) Improved prediction of signal peptides: SignalP 3.0. *J Mol Biol* 340(4):783–795.
43. Herzig V, et al. (2011) ArachnoServer 2.0, an updated online resource for spider toxin sequences and structures. *Nucleic Acids Res* 39(Database issue):D653–D657.
44. Klint JK, et al. (2013) Production of recombinant disulfide-rich venom peptides for structural and functional analysis via expression in the periplasm of *E. coli*. *PLoS One* 8(5):e63865.
45. Mobli M, Stern AS, Bermel W, King GF, Hoch JC (2010) A non-uniformly sampled 4D HCC(CO)NH-TOCSY experiment processed using maximum entropy for rapid protein sidechain assignment. *J Magn Reson* 204(1):160–164.
46. Güntert P (2004) Automated NMR structure calculation with CYANA. *Methods Mol Biol* 278:353–378.
47. Fletcher JI, Chapman BE, Mackay JP, Howden ME, King GF (1997) The structure of versutoxin (δ-atracotoxin-Hv1) provides insights into the binding of site 3 neurotoxins to the voltage-gated sodium channel. *Structure* 5(11):1525–1535.
48. Shen Y, Delaglio F, Cornilescu G, Bax A (2009) TALOS+: A hybrid method for predicting protein backbone torsion angles from NMR chemical shifts. *J Biomol NMR* 44(4):213–223.
49. Davis IW, et al. (2007) MolProbity: All-atom contacts and structure validation for proteins and nucleic acids. *Nucleic Acids Res* 35(Web Server issue):W375-83.
50. McCarthy CA, Vinh A, Callaway JK, Widdop RE (2009) Angiotensin AT_2 receptor stimulation causes neuroprotection in a conscious rat model of stroke. *Stroke* 40(4):1482–1489.